A&A 461, 205–214 (2007)
DOI: 10.1051/0004-6361:20065070
© ESO 2006

Astronomy & Astrophysics

Time-dependent H_2 formation and protonation in diffuse clouds

H. S. Liszt

National Radio Astronomy Observatory, 520 Edgemont Road, 22903-2475 Charlottesville, VA, USA
e-mail: hliszt@nrao.edu

Received 22 February 2006 / Accepted 14 September 2006

ABSTRACT

Aims. To demonstrate the time-approach to equilibrium of H_2-formation and protonation in models of diffuse or H I interstellar gas clouds previously published by the author.

Methods. The microscopic equations of H_2-formation and protonation are integrated numerically over time in such a manner that the overall structures evolve self-consistently under benign conditions.

Results. The equilibrium H_2 formation timescale in an H I cloud with $N(\mathrm{H}) \approx 4 \times 10^{20}$ cm^{-2} is $1-3 \times 10^7$ yr, nearly independent of the assumed density or H_2 formation rate on grains, etc. Attempts to speed up the evolution of the H_2-fraction would require densities well beyond the range usually considered typical of diffuse gas. The calculations suggest that, under benign, quiescent conditions, H_2 in the diffuse ISM formation of H_2 is favored in larger regions having moderate density, consistent with the rather high mean kinetic temperatures measured in H_2, 70−80 K.

Formation of H_3^+ is essentially complete when H_2-formation equilibrates but the final abundance of H_3^+ appears more nearly at the very last instant. Chemistry in a weakly-molecular gas has particular properties so that the abundance patterns change appreciably as gas becomes more fully molecular, either in model sequences or with time in a single model. One manifestation of this is that the predicted abundance of H_3^+ is much more weakly dependent on the cosmic-ray ionization rate when $n(H_2)/n(H) \lesssim 0.05$. In general, high abundances of H_3^+ do not enhance the abundances of other species (e.g. HCO^+) but late-time OH formation proceeds most vigourously in more diffuse regions having modest density, extinction and H_2 fraction and somewhat higher fractional ionization, suggesting that atypically high OH/H_2 abundance ratios might be found optically in diffuse clouds having modest extinction.

Key words. ISM: molecules – ISM: atoms – ISM: clouds

1. Introduction

The fact that individual H I/diffuse clouds have a substantial component of molecular hydrogen has been recognized observationally since the original *Copernicus* observations (Jura 1974; Spitzer 1978) and a quite high fraction of hydrogen in the nearby diffuse interstellar medium (ISM) overall is in molecular form (Savage et al. 1977; Liszt & Lucas 2002). More surprising perhaps is the recent discovery that this molecular component hosts a rich polyatomic chemistry with relatively large amounts of H_3^+ (McCall et al. 2002) and a dozen other species including such ions as HCO^+ (Lucas & Liszt 1996) and HOC^+ (Liszt et al. 2004) and molecules as complex as C_3H_2 (Cox et al. 1988; Lucas & Liszt 2000), H_2CO (Liszt & Lucas 1995; Moore & Marscher 1995; Liszt et al. 2002) and NH_3 (Nash 1990; Liszt et al. 2002).

The presence of copious H_2 and relatively large amounts of H_3^+ in H I clouds is supported theoretically when self-shielding (Lee et al. 1996) is included in equilibrium models of diffuse gas (Liszt & Lucas 2000; Liszt 2003) using empirically-determined H_2 formation rates (Jura 1974; Spitzer 1978; Gry et al. 2002); observed HD/H_2 ratios are also explained as long as the cosmic-ray ionization rate is taken large enough to support the inferred proton density in the presence of atomic-ion neutralization on small grains. However, formation of H_2 is a notoriously slow and supposedly rather fragile process. Moreover, it remains to be determined whether any such equilibrium is actually attained in the interstellar medium, which is the subject of this work.

Here we show the approach to equilibrium in the models discussed by Liszt & Lucas (2000), Liszt (2002) and Liszt (2003): we present calculations of time-dependent H_2 and H_3^+ formation in small, mostly-static gas parcels meant to represent typical diffuse "clouds", like, for instance, the "standard" H I cloud of Spitzer (1978). As we discuss, the distinguishing characteristic of the chemistry in such clouds is that the H_2 formation process is unsaturated ($n(H_2) < n(H)/2$). For this reason the equilibrium timescales for H_2 formation cannot be calculated from simple scaling arguments based on the local microscopic H_2 formation rate, nor are they shortened by self-shielding, or in many cases by assuming higher density or even a higher rate constant for H_2 formation on grains, etc. Furthermore the abundance of H_3^+ does not always vary as might be expected from consideration of its equilbrium chemistry in more fully molecular gas.

Section 2 gives details of the methods used in the calculations, results of which are presented and discussed in Sects. 3 and 4.

2. Details of the calculations and microphysics

2.1. Framework and initial conditions

The calculations presented here build on a framework which was established in the work of Wolfire et al. (1995). Specifically, the two-phase model of heating and cooling developed by Wolfire et al. (1995) (see also Wolfire et al. 2003) was applied to small, uniformly illuminated spherical gas clots of constant density, intended to represent diffuse "clouds"; our model, however, uses the gas-phase abundances of Savage & Sembach (1996) which makes them a bit hotter. Assumption of a geometry is required

Article published by EDP Sciences and available at http://www.aanda.org or http://dx.doi.org/10.1051/0004-6361:20065070

because the accumulation of H_2 and CO depends on shielding by dust and other molecules and is, therefore, strongly nonlinear. We used the shielding factors calculated by Lee et al. (1996). Typical densities and column densities considered here, $n(\mathrm{H}) = 32$ cm^{-3}, $N(\mathrm{H}) = 4\times10^{20}$ cm^{-2} correspond to a Spitzer "standard cloud" (Spitzer 1978) having a dimension of a few pc and median reddening 0.05 mag over the face of the cloud. The central column density in such an H I cloud corresponds to the regime where the appearance of high H_2-fractions is first noted in the ISM.

In general, the hydrogen densities in our models (number or column) are assumed values. The temperature and thermal pressure follow from the details of the calculation, chiefly through the assumed gas-phase abundances of the dominant coolants carbon and oxygen, and the influence of the radiation field in heating the gas via the photoelectric effect on the same small grains which are so largely responsible for the overall charge balance. As shown in Fig. 9 of Liszt & Lucas (2000), a given value of the scaling factor (G_0) for the overall radiation field produces a roughly constant thermal pressure in the outer regions of our models, increasing somewhat with assumed density and decreasing slightly going inward from the cloud edge. The generally-accepted value for the thermal pressure of the ISM, $p/k \approx 2{-}3\times10^3$ cm^{-3} K (Jenkins 2002; Jenkins & Tripp 2001) indeed applies to our typical model of the Spitzer "standard cloud" and the very densest models considered here have pressures a factor 2−3 times higher, as seems observationally to be the case as well.

The initial condition here is simply the equilibrium diffuse cloud model which would be calculated in the absence of any molecular chemistry, as is more typical in discussions of the overall structure of the diffuse ISM (Wolfire et al. 2003). That is, the initial model is equilibrated and self-consistent in terms of thermal and ionization equilibrium, but no molecule formation has occurred. Our models include the rudiments of molecular chemistry as discussed in several recent papers concerning questions of equilibrium CO, H_2, HD and H_3^+ formation in diffuse gas (Liszt & Lucas 2000; Liszt 2002, 2003). Incorporation of the chemistry should not normally upset the basic microphysical balance (ionization, thermodynamic, etc.) in diffuse gas because such small fractions of oxygen and carbon are sequestered, although inclusion of OH and H_2 formation can affect some aspects of the distribution of charge among species.

Another effect mitigating the influence of H_2 formation in diffuse gas is the dominance of atomic-ion neutralization by small grains, substantially lowering the H^+ and electron density which would otherwise obtain in the presence of cosmic-ray ionization of hydrogen (Wolfire et al. 1995; Liszt 2003). This effect is of the utmost importance in understanding the interplay between the cosmic ray ionization rate ζ_{H} (here taken as the rate per free H-nucleus) and abundance of H_3^+ (Liszt 2003) . Detailed calculation including grain charging (Draine & Sutin 1987; Weingartner & Draine 2001) is required if the heating rate is to be properly calculated according to the prescription of Bakes & Tielens (1994).

2.2. Formation of H_2

In this work we distinguish between the *formation* of H_2, which we consider to be a microscopic physical effect occuring on individual large grains and involving individual or paired H-atoms, and the *accumulation* of H_2 in the ISM, which is a macroscopic effect involving assumptions about cloud geometry, ISM topology, and so forth. The purpose of this work is to understand the macroscopic aspects of the accumulation of H_2 in the ISM and we employ only the most standard, empirical, microscopic description of its formation.

That is, the volume formation rate of H_2 is expressed as $\mathrm{d}n(\mathrm{H}_2)/\mathrm{d}t = n(\mathrm{H})\, n(\mathrm{H\,I})\, R_{\mathrm{G}}\, \langle v_{\mathrm{T}}\rangle = 3\times10^{-18}$ cm^3 s^{-1} $n(\mathrm{H})\, n(\mathrm{H\,I})\, \sqrt{T_{\mathrm{K}}}$ (Spitzer 1978) where the factor $n(\mathrm{H})$ (the total density of H-nuclei) represents a constant number of large H_2-forming grains per H-nucleus in the gas; $n(\mathrm{H\,I})$ is the density of atomic hydrogen (after protons, H^- ions, and H_2, etc. are reckoned) and the thermal velocity and/or kinetic temperature terms correspond to the speed at which H-atoms move through the gas, possibly encountering large grains. The rate constant R_{G} nominally includes a sticking coefficient.

The inferred rate in the diffuse ISM has been remarkably steady over the last 25 years (Jura 1974; Spitzer 1978; Gry et al. 2002) and use of this simple formulation, combined with the modern shielding coefficients, accounts extremely well for the observations of H_2 in diffuse lines of sight (Liszt & Lucas 2000). As discussed in Sect. 3 (see Fig. 4) varying the assumed value of R_{G} by factors of a few has appreciable effect upon the amount of H_2 which is produced but the equilibrium time scale changes little. As an aside we note that the gas-phase formation of H_2 via H^-, which could account for some of the very low molecular fractions seen along lines of sight having low extinction (Liszt 2002), is included in the present calculations as well but without much effect.

2.3. Solving the H_2-accumulation problem

The equilibrium solutions for the radial distributions of CO, H_2 and H_3^+ described in our earlier papers were achieved through what is essentially a relaxation method. An initially atomic sphere is divided into a substantial number (typically 100) of thin radial shells and the molecular densities are calculated for each, working inward, self-consistently accounting for the shielding which accrues from each configuration. Each time a quasi-equilibrium state is reached for the entire structure (that is, when the calculation has successively converged in each shell), the calculation starts anew at the outermost shell (whose H_2-abundance was, after all, calculated in at least partial ignorance of the conditions interior to it) and the process is repeated until the whole structure varies sufficiently little between iterations. The process is not particularly difficult or unstable and convergence is rapid, typically requiring only a few seconds on a recent laptop computer. Note that the thermal and charge balance, etc. are continually updated during the calculation.

The time-dependent calculations basically just wrap the equilibrium solver in an outer loop which allows the entire structure to evolve self-consistently over short times. The time step, which initially cannot be as large as even 1000 years in most cases, is examined and lengthened by a factor of $\sqrt{2}$ whenever the structure changes sufficiently little between time steps. The full time-dependent calculation *is* somewhat tedious, typically requiring several hours per model and much exercising of the tiny (but assertive) fan on the author's laptop computer in cases of high H_2-fraction.

2.4. Elementary analytic considerations of the time-dependent solutions for H_2

Although the real solution to the time-dependent accumulation problem is strongly non-linear and can only be achieved globally over an entire geometrical construct, several important aspects

of the problem may be understood with reference to a simple parametric treatment of purely local behaviour.

Accordingly, the local rate of accumulation of molecular hydrogen may be written

$$d\mathrm{n}(\mathrm{H_2})/d\mathrm{t} = -n(\mathrm{H_2})\Gamma_{\mathrm{H_2}} + R_{\mathrm{G}} n(\mathrm{H}) n(\mathrm{H\,I}) \sqrt{T_{\mathrm{K}}} \quad (1)$$

where $\Gamma_{\mathrm{H_2}}$ is the rate of H_2 destruction (mostly by cosmic rays and ultra-violet photons, although interaction of He^+ and H_2 is included in the numerical calculation), T_{K} is the kinetic temperature (calculated in the models) and $R_{\mathrm{G}} = 3 \times 10^{-18}$ cm^3 s^{-1} (see Sect. 2.2). After rewriting $n(\mathrm{H\,I}) = n(\mathrm{H}) - 2n(\mathrm{H_2})$ (for the present purposes; all forms of hydrogen are considered in the numerical models) the solution is

$$n(\mathrm{H_2})_{|t} = b/a + (n(\mathrm{H_2})_{|t=0} - b/a)\mathrm{e}^{-at} \quad (2)$$

where $a = \Gamma_{\mathrm{H_2}} + 2R_{\mathrm{G}} n(\mathrm{H}) \sqrt{T_{\mathrm{K}}}$, $b = R_{\mathrm{G}} n(\mathrm{H})^2 \sqrt{T_{\mathrm{K}}}$.

The time constant in the problem is $1/a$, where a is a linear combination of the per-particle formation and destruction rates, observing the conservation of H-nuclei, and is therefore relatively short in weakly-shielded gas. The rate of accumulation of H_2 takes on its highest value $\mathrm{d}n(\mathrm{H_2})/\mathrm{d}t = b$ at time 0 and the equilibrium solution $n(\mathrm{H_2})_{|t\to\infty} = b/a$ may be thought of as the result of accumulation at the maximum rate over a period of time $1/a$. Thus, self-shielding (lowering $\Gamma_{\mathrm{H_2}}$) cannot increase the rate at which H_2 forms or speed up the accumulation of H_2, it only increases the final amount of H_2 by allowing the accumulation process to work longer. By lengthening the time-scale, self-shielding may also provide a buffer against sudden change once equilibrium is attained.

Increasing the microscopic formation rate constant or density will hasten the pace at which H_2 accumulates but even so, global equilibria are not generally achieved more rapidly in cases where the H_2 fraction would otherwise be small, as discussed in Sect. 3 (see Fig. 4); it only happens that more H_2 is made (which requires somewhat more time). Maintenance of high equilibrium H_2-fractions requires $\Gamma_{\mathrm{H_2}} \lesssim R_{\mathrm{G}} n(\mathrm{H}) \sqrt{T_{\mathrm{K}}}$, which is roughly equivalent to reducing the photodestruction rate (of order 10^{-10} s^{-1} in free space) to insignificance i.e. $\Gamma_{\mathrm{H_2}} \approx \zeta_{\mathrm{H}}$.

2.5. Weak vs. slow processes

Indeed, the situations which equilibrate most rapidly are those for which the H_2 abundance is smallest, which exemplifies the fact that even processes like H_2 formation or cosmic-ray ionization – which seem weak because they have low rates – may equilibrate quickly when not called upon to do very much; the time constant is then determined by the overall destruction rate, which may be high. It is for this reason that formation of H_3^+ – a much higher-order process which after all requires formation of H_2, cosmic ray ionization of H_2 and further interaction of H_2^+ and H_2 (see Sect. 4.2) – is essentially complete as soon as H_2 accumulation equilibrates: one need not wait for a further period $1/\zeta_{\mathrm{H}}$.

2.6. The cosmic-ray ionization rate ζ_{H}

The evolution of the H_2 fraction is largely independent of the assumed value of ζ_{H} in our models but the standard cosmic-ray ionization rate assumed in the models in this work is $\zeta_{\mathrm{H}} = 10^{-16}$ s^{-1} (the cosmic-ray destruction rate per H_2 is slightly more than $2\zeta_{\mathrm{H}}$). This is approximately one order of magnitude larger than what is often used in calculations of cosmic-ray ionization of the ISM (Wolfire et al. 1995) especially for dense dark cloud chemistry and is about that which is needed to explain the overall abundance of H_3^+ (see Sect. 4). The equilibrium H_3^+ concentration is nearly proportional to ζ_{H} in our models having larger H_2 fractions (see Fig. 5) owing to the intervention of small-grain neutralization of protons: the formation can be pushed harder without unduly increasing the electron density and recombination rate for H_3^+. However, for reasons discussed in Sect. 4, the concentration of H_3^+ is more weakly dependent on ζ_{H} in regions of small H_2-fraction or when ζ_{H} is very large.

2.7. Heating by cosmic rays and H_2-formation

The current assumption is that the diffuse ISM is heated by the photoelectric effect on small grains in both the warm phase (where X-rays make a larger contribution) and cool phase. The heating rate as a function of density in partly-shielded gas is shown in Fig. 3 of Wolfire et al. (1995) based on the work of Bakes & Tielens (1994). As may be seen from that figure, the cosmic ray heating rate is roughly 1.2 dex below that of the photoelectric effect in diffuse gas and 2−2.5 dex lower in cool gas, for $\zeta_{\mathrm{H}} = 10^{-17}$ s^{-1}. Thus the higher cosmic-ray ionization rates considered here may imply a substantial contribution to the heating of the warm gas by cosmic rays, harkening back to the very earliest discussions of two-phase equilibrium, before the role of diffuse X-ray heating was incorporated (Goldsmith et al. 1969). The highest cosmic-ray rates considered here still do not produce dominant heating effects in the cool neutral gas, but much higher ionization rates $\zeta_{\mathrm{H}} \gtrsim 10^{-15}$ s^{-1} were recently suggested by Le Petit et al. (2004) for the line of sight to ζ Persei.

In our models there is a modest contribution to the heating due to H_2 formation, comparable to that arising from heating by cosmic-ray ionization of H I. The volume heating rate due to the latter is $\zeta_{\mathrm{H}}\, n(\mathrm{H\,I}) \langle E_{\mathrm{cr}} \rangle$ where $\langle E_{\mathrm{cr}} \rangle \approx 8$ eV is the energy available for heating after the primary ionization. The equivalent rate for H_2-formation is $R_{\mathrm{G}} n(\mathrm{H}) n(\mathrm{H\,I}) \sqrt{T_{\mathrm{K}}} \langle E_{\mathrm{H_2}} \rangle$ where $\langle E_{\mathrm{H_2}} \rangle$ represents that fraction of the heat of formation of H_2 which is available to heat the gas. The heating rates for the two processes are very nearly equal under typical conditions, $\zeta_{\mathrm{H}} = 10^{-16}$ s^{-1}, $T_{\mathrm{K}} = 80$ K, $n(\mathrm{H}) = 32$ cm^{-3} and $\langle E_{\mathrm{H_2}} \rangle = 1.5$ eV.

2.8. The recombination rate of H_3^+ and other chemical reactions

The chemical rate constants used in our models have been taken from the UMIST database (Le Teuff et al. 2000) (see `http://www.rate99.co.uk`) including, for consistency with the results of Liszt (2003), the rate constant for $e + H_3^+$ recombination $\alpha(T_{\mathrm{K}}) = 4 \times 10^{-6}/\sqrt{T_{\mathrm{K}}}$ cm^3 s^{-1}. This rate has been measured many times, including, most recently and probably accurately, by McCall et al. (2003). Their measured values, at 23 K and 300 K, are 70% of those used in our work.

3. Time-dependent H_2 accumulation in diffuse clouds

3.1. Evolutionary effect of varying column density

Figure 1 shows the evolution of the H_2 and H_3^+ densities in a series of models, each having the same uniform total density of hydrogen $n(\mathrm{H}) = 32$ cm^{-3} threaded by a cosmic ray flux yielding $\zeta_{\mathrm{H}} = 10^{-16}$ s^{-1}. The central column density of hydrogen across the clouds $N(\mathrm{H})$ (from edge to edge) varies from 0.5 to 16×10^{20} cm^{-2}, as indicated at the right hand side of each

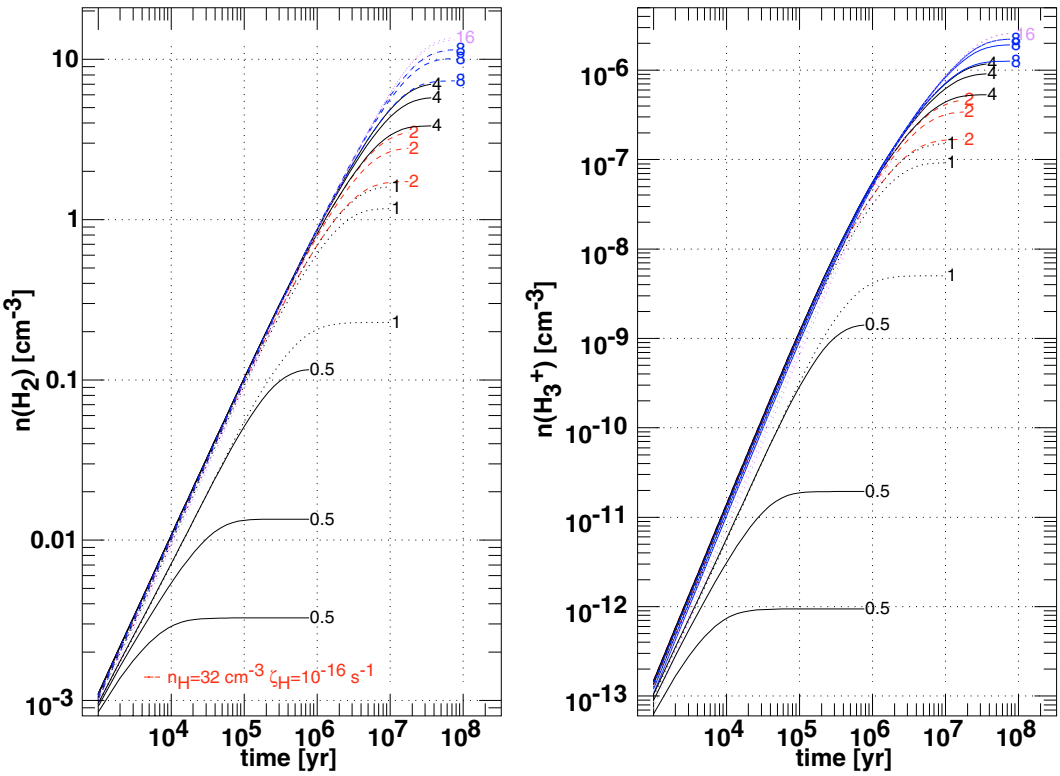

Fig. 1. Density of molecular hydrogen $n(H_2)$ (*left*) and H_3^+ (*right*) as functions of time within spherical, uniformly illuminated, initially atomic gas spheres of constant density of H-nuclei $n(H) = 32$ cm^{-3}, threaded by a cosmic ray flux yielding a primary ionization rate per H-atom $\zeta_H = 10^{-16}$ s^{-1}. Three curves corresponding to shells at fractional radii 0, 1/3 and 2/3 from the center are shown for each of a series of models with differing central column density of hydrogen 0.5×10^{20} cm^{-2} $\leq N(H) \leq 16 \times 10^{20}$ cm^{-2}. The physical size of the models in pc and their central (edge-to-edge) column density in units of 10^{20} cm^{-2} are equal and shown at the right of each curve.

curve. The physical size of the models (diameter) in pc is, coincidentally, equal to the column density as labelled in units of 10^{20} cm^{-2}. Three curves are shown for each model, corresponding to the shells centered at fractional radii 0, 1/3 and 2/3 from the center. These curves separate at larger times when the outermost regions have reached equililbrium. For a sphere, the median line of sight occurs at a fractional impact parameter of 2/3 where the column density traversed is 3/4 that at the center. The median line of sight through the model with central column density 4×10^{20} cm^{-2}, 3×10^{20} cm^{-2} corresponds exactly to the standard H I cloud of Spitzer (1978).

For the optically-thinnest model there is a large radial gradient in the H_2 density and a wide disparity between the times required to reach equilibrium (10^4–10^6 yr). The fact that such appreciable (easily detectable) amounts of H_2 form in as little as 10^4 yr demonstrates why it is so hard to find lines of sight having measurable reddening which are devoid of H_2. For $N(H)$ as large as 16×10^{20} cm^{-2} the H_2 accumulation process is thoroughly saturated ($n(H_2) \rightarrow n(H)/2$) when equilibrium is reached at very large times approaching 10^8 yr. Models in which the equilibrium H_2-distribution is more uniform also evolve more uniformly, as illustrated in Fig. 2 which shows (at top) the time-dependent evolution of the radial variation of $n(H_2)$ in the model resembling a "standard" H I cloud. The H_2-density is remarkably constant for fractional radii of 90% or more for most of the first 1–3×10^6 yr, after which a more molecular core develops, as well as a very thin (actually, unresolved) transition layer into a more nearly atomic envelope.

Clearly, self-shielding is important only at somewhat later times. In some models with moderate density, $n(H_2)$ behaves as a single power-law from center to edge, as illustrated in Fig. 2 at bottom which shows the equilibrium solutions for $n(H_2) = 32$ cm^{-3} corresponding to the models used in Fig. 1. However this is not a general feature of the equilibrium solutions. Figure 2 also illustrates the effect of finite resolution on the structure of the atomic envelope, which fractionally is substantially larger with higher resolution. The results in Fig. 1 are not affected by the illustrated doubling of the number of radial shells.

As shown in Fig. 1, even a standard H I cloud model has a very substantial fraction of molecular hydrogen in its interior. This of course is borne out observationally (Jura 1974) as molecular fractions of 25–45% are derived for even the diffuse ISM observed in *uv*/optical absorption lines of H_2 and CH (Savage et al. 1977; Liszt & Lucas 2002). Less obvious, however, is that the conditions so favourable to H_2 may actually work for as long as the calculations require to reach equilibrium in Fig. 1, i.e. for times as long as 10^8 yr.

3.2. Evolutionary effect of varying number density

It seems natural to inquire in what ways the evolution might be hastened. Shown in Fig. 3 are results for series of models of different number density 8 cm^{-3} $\leq n(H) \leq$ 128 cm^{-3} at column densities $N(H) = 2$–16×10^{20} cm^{-2}. At least for moderate column densities, as shown at the left in Fig. 3, increasing the number density within the range expected for diffuse gas has surprisingly little effect on the time required for the models to reach equilibrium: the increased rate of accumulation is compensated by the tendency to produce more H_2, making the equilibrium

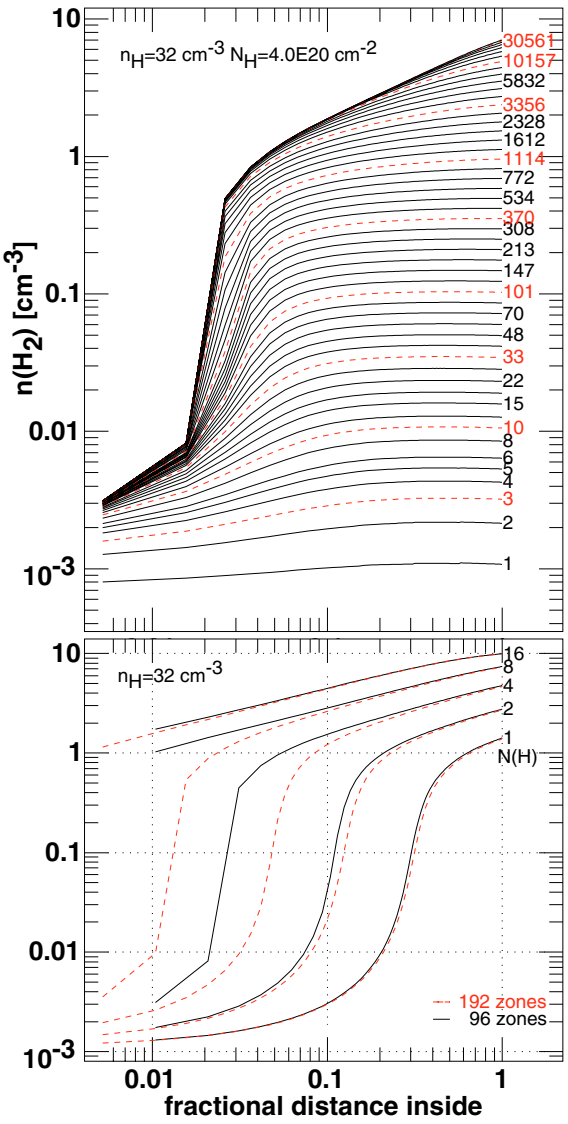

Fig. 2. Radial and secular variation of molecular hydrogen density within models illustrated in Fig. 1. *Top*: time evolution of $n(H_2)$ for $n(H) = 32$ cm^{-3}, $N(H) = 4 \times 10^{20}$ cm^{-2}. Labels at right give the elapsed time in units of 1000 yr. *Bottom*: radial variation in equilibrium for $n(H) = 32$ cm^{-3} and $N(H) = 1, 2, 4, 8, 16 \times 10^{20}$ cm^{-2}, for calculations employing 96 and 192 radial zones.

timescale about constant over a wide range of density for the standard H I cloud column density.

Only when very high H_2 fractions are attained at a given density does increasing the density shorten the equilibrium time (i.e. Fig. 3 at right, or for the two very highest densities at left). With reference to Fig. 3, note that, although the local accumulation rate initially varies as $n(H)^2 \sqrt{T_K} \propto n(H)^{3/2}$ in thermal pressure equilibrium, the total amount of H_2 produced within a model at any time is much less dependent on density because the more tenuous models are larger, varying as $1/n(H)$. Obviously, all models in which the H_2 accumulation saturates at high molecular fractions produce the same $N(H_2)$ if they have the same $N(H)$, so less dense models having the same $N(H_2)$ then make more H_2 molecules overall because they are larger.

3.3. Does size matter?

Physically larger clouds tend to produce more H_2 in both series of models just discussed. Those in Fig. 1 with larger column density $N(H)$ are physically larger and have higher internal molecular number density, so, at fixed number density, physically larger regions of higher column density are responsible for the very great bulk of the accumulation of H_2. In Fig. 3, molecular number densities are higher in clouds of higher $n(H)$, but usually not by such large amounts as to compensate for the very large differences in volume. That is, the model volumes vary by a factor $(128/8)^3 \approx 4000$ whereas $n(H_2)$ varies by factors of 100−500 for the models with $N(H) = 4{-}16 \times 10^{20}$ cm^{-2}. Over a substantial range in $N(H)$, it is expected that the bulk of the molecules will form in (again) physically larger regions, but of lower density.

So is the bulk of the interstellar H_2 really formed in large tenuous regions, or in more compact, denser ones? Observationally, the mean column density-weighted kinetic temperature inferred for H_2-forming diffuse gas is 70−80 K (Savage et al. 1977; Shull et al. 2004), which, for typical interstellar thermal pressures, implies densities like those of the standard H I cloud[1]. Attempts to form the observed H_2 more rapidly in regions of high density must account for these high kinetic temperatures; perhaps it is relevant that Jenkins & Tripp (2001) found a small but pervasive fraction of material at much higher than normal thermal pressure in typical diffuse clouds probed in the fine-structure excitation of C I. This high-pressure component is generally ignored in calculation of the mean thermal pressure in the ISM, but would approximately double it.

3.4. Changes in formation and dissociation rate constants

The empirically-inferred microscopic formation rate of molecular hydrogen formation has changed remarkably little since H_2 was first observed in the ISM (Jura 1974; Spitzer 1978; Gry et al. 2002). Figure 4 shows the effects of changing the assumed H_2 formation rate constant R_G in some of the models illustrated in Fig. 1. Although the H_2 column and number densities increase faster than linearly with changes in R_G at late times, the timescale may only be shortened after the molecular fraction approaches its maximum possible value.

As noted in Sect. 2.4, high molecular fractions may only accrue in cases where the free-space photodissociation rate of H_2 is attenuated (by dust and self-shielding) to the point where it is no more than competitive with cosmic-ray induced destruction rates. It follows that natural variations in the ambient interstellar radiation field (ISRF) may encourage or discourage H_2 accumulation, but only modestly and at late times when equilibrium is approached. Shown in Fig. 5 at left are results for a lower-density model ($n(H) = 8$ cm^{-3}) at $N(H) = 4 \times 10^{20}$ cm^{-2}, with the ISRF lowered by factors of 2 and 4. Clearly the H_2 accumulation process may be enhanced by making the material sufficiently dark, but only at the expense of incurring very long equilibrium times. Note that the darker models actually form and accumulate somewhat less H_2 at smaller times because they are substantially cooler; lower photoelectic heating rates accompany lower photoionization rates for molecules. Clouds in very locally darker regions would have to be overpressured in order to compensate for this sluggishness, but in the ISM a tendency to higher thermal pressure at higher density seems a real effect.

[1] Note that the surveys from which these mean temperatures are derived have somewhat low sample mean H_2-fractions, 0.17−0.18.

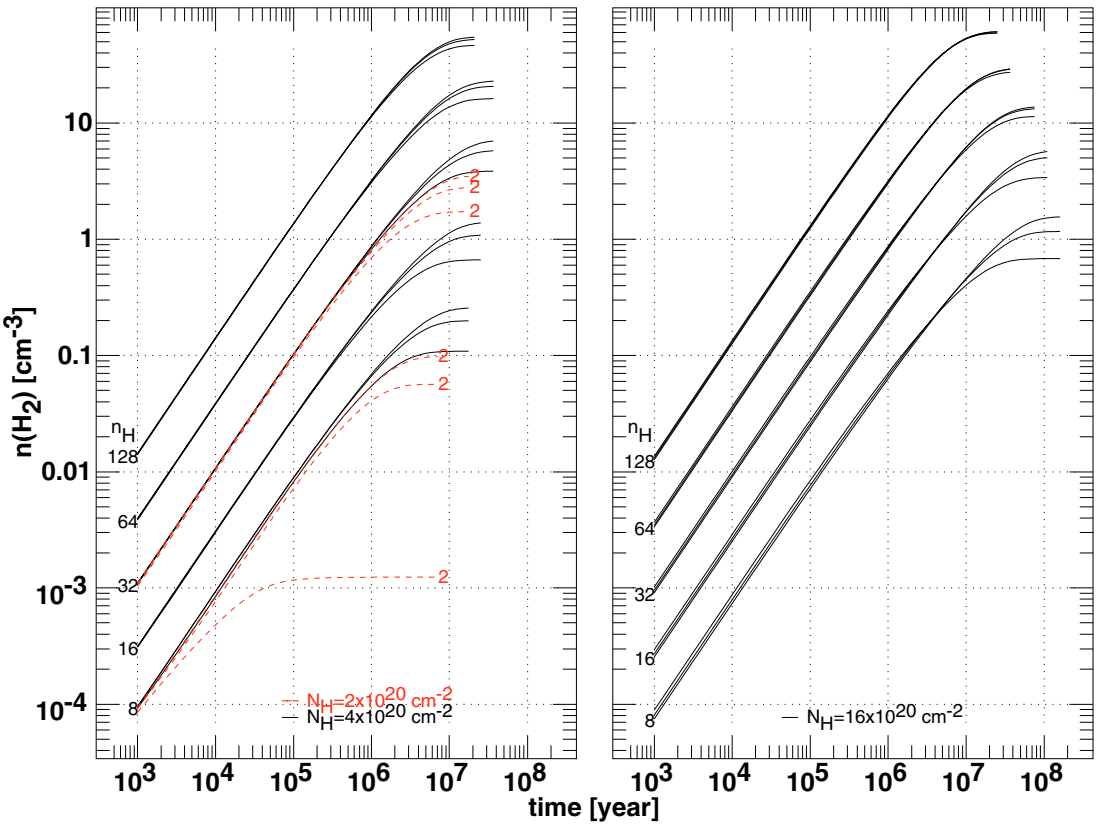

Fig. 3. Density of molecular hydrogen $n(H_2)$ as a function of time within spherical, uniformly illuminated, initially atomic gas spheres of differing density of H-nuclei $n(H) = 8-128$ cm^{-3} (as shown at the left of each family of curves), threaded by a cosmic ray flux yielding a primary ionization rate per H-atom $\zeta_H = 10^{-16}$ s^{-1}. *At right*, all models have a central column density $N(H) = 16 \times 10^{20}$ cm^{-2} (from edge to edge); *at left*, results are interspersed for $N(H) = 2$ (dashed; red in appropriate media) and 4×10^{20} cm^{-2}. As in Fig. 1, three curves are shown for each model, corresponding to fractional radii 0, 1/3 and 2/3 from the cloud center.

Figure 5 at right shows the effect of varying the primary cosmic ray ionization rate by factors of three about the standard value $\zeta_H = 10^{-16}$ s^{-1}. Such variations have little effect on the equilbrium H_2 densities in standard H I clouds as long as they are not so large as to upset the thermal balance (which can occur for $\zeta_H \gtrsim 10^{-15}$ pc). The more complicated behaviour of H_3^+ is discussed in Sect. 4.

4. H_3^+ and other trace species

4.1. Evolution of $n(H_3^+)$

In the ISM there is a general increase in $N(H_3^+)$ with reddening corresponding to $N(H_3^+) = 8 \times 10^{14}$ cm^{-2} over 6 mag, or to $N(H_3^+)/N(H) \approx 2.3 \times 10^{-8}$ for the standard gas-reddening ratio $N(H)/E_{B-V} = 5.8\times10^{21}$ cm^{-2} mag^{-1} (see Fig. 14 of McCall et al. 2002).

As discussed previously (Liszt 2003) or as shown in the figures here, $n(H_3^+)$ concentrations comparable to those required can be produced in equilibrium models of diffuse clouds of moderate number and column density for cosmic ray ionization rates ζ_H at or somewhat above 10^{-16} s^{-1} (see Fig. 5 at right). Such models of H_3^+ in diffuse gas have the added virtue that the HD/H_2 ratios observed in diffuse clouds – which are very sensitive to the actual proton density – are also reproduced.

As shown in the figures, the H_3^+ fraction is sensitive to the same effects which increase the concentration of H_2, and in some circumstances to the cosmic ray ionization rate as well (Fig. 5 here). There are some more subtle effects which are less obvious in the figures: in models which achieve large H_2-fractions, the electron density is lower by a factor of (typically) about two at late times because the gas cannot sustain high proton densities when most of the hydrogen is molecular.

Although the H_3^+ fraction equilibrates on very much the same final timescale as that of H_2, the problem of timescales is somewhat more critical for H_3^+ because its time derivative is much steeper; the final concentration occurs more nearly at only the final moments of the calculation. Conversely, the H_3^+ fraction would deteriorate more rapidly should conditions suddenly become less hospitable. Of course this effect is mitigated slightly when the H_3^+ fraction is calculated with respect to H_2 (instead of $n(H)$) but in most cases the lines of sight with known $N(H_3^+)$ are not accessible to direct measurement of $N(H_2)$ or even $N(H\,I)$. Note that H_3^+ is also more centrally concentrated than H_2, but the effect is really strong only in models within which there are larger radial gradients in $n(H_2)$.

4.2. Effect of changing ζ_H

The presence of high cosmic ray ionization rates in diffuse gas has been inferred from very elementary analysis of the H_3^+ abundance which treats it like an atomic ion (McCall et al. 2002). Assuming – as is true of dark, dense molecular gas – that every primary ionization of H_2 leads to an H_3^+ ion and that H_3^+ ions are destroyed by electron recombination with a rate

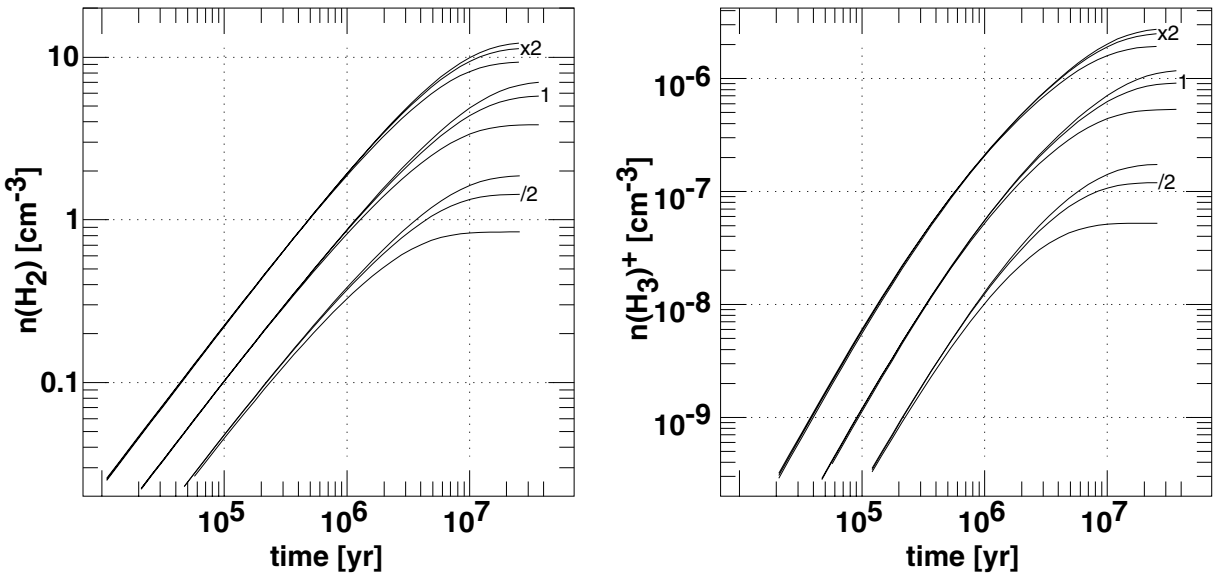

Fig. 4. Similar to Fig. 1, for models having $n(\mathrm{H}) = 32$ cm^{-3}, $N(\mathrm{H}) = 4 \times 10^{20}$ cm^{-2} and primary cosmic ray ionization rate $\zeta_\mathrm{H} = 10^{-16}$ s^{-1}, with the rate constant for H_2 formation scaled by factors of 2 about the standard value.

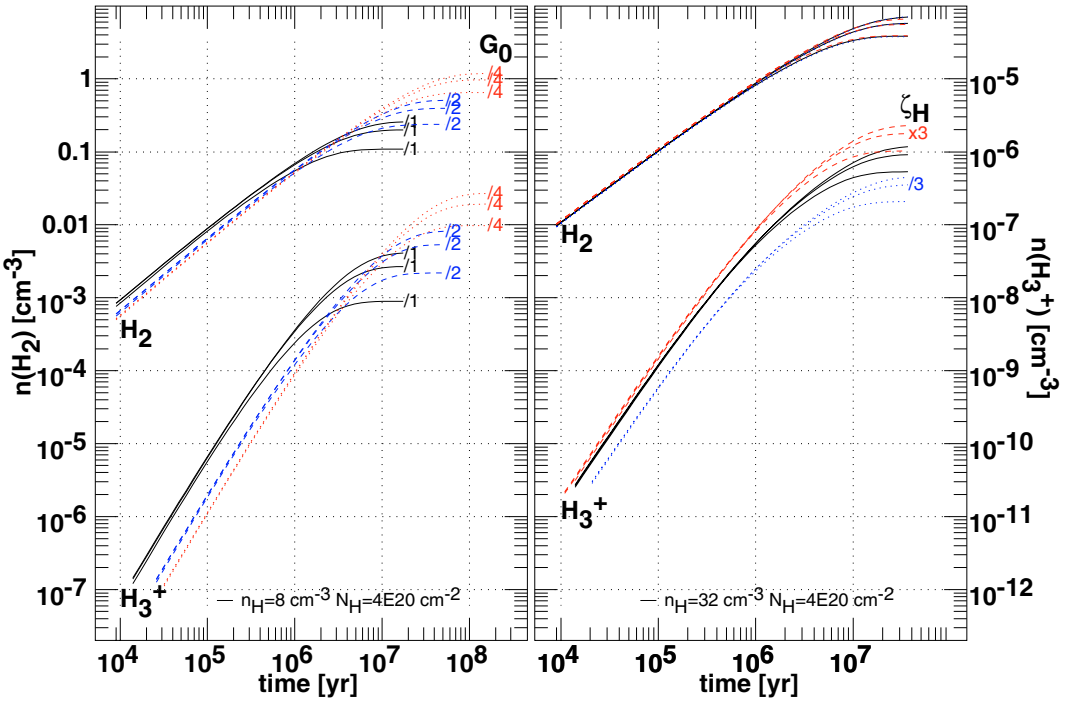

Fig. 5. H_2 and H_3^+ densities calculated for varying strengths of the interstellar radiation field (*left*) and cosmic ray primary ionization rate ζ_H (*right*): the scale for $n(H_2)$ is given at far left, that for $n(H_3^+)$ at far right. In the panel at left the scaling parameter G_0 is taken as 1, 1/2 and 1/4; at right ζ_H varies by factors of 3, 1 and 1/3 about the standard model value $\zeta_\mathrm{H} = 10^{-16}$ s^{-1}. As in Fig. 1, three curves are shown for each model, at fractional radii 0, 1/3, and 2/3 from the center. The models in both panels have $N(\mathrm{H}) = 4 \times 10^{20}$ cm^{-2} but the model at left has lower number density $n(\mathrm{H}) = 8$ cm^{-3}. Note that $n(H_3^+)$ is relatively insensitive to changes in ζ_H at early times when $n(H_2)$ is small, as discussed in Sect. 4 of the text.

constant α_e, there follows a simple, formal expression for the H_3^+ density:

$$n(\mathrm{H_3^+}) \approx 2\zeta_\mathrm{H} n(\mathrm{H_2})/(\alpha_e\, n(\mathrm{e})). \quad (3)$$

The discrepancy between observation and the values of $n(H_3^+)$ which result from putting typical values for ζ_H, $n(\mathrm{e})$, etc. in this expression is sufficient to suggest that $\zeta_\mathrm{H} \gg 10^{-17}$ s^{-1}. Nonetheless, Eq. (3) is only a formal, very approximate solution for $n(H_3^+)$ because of the implicit dependences of $n(\mathrm{e})$ and α_e upon the physical effects of ionization and heating (respectively) denoted by ζ_H, and because of other, less obvious assumptions made about the molecular chemistry. Furthermore, the obvious changes in the H_3^+/H_2 ratio with time show that such considerations might at best apply only at very late times (e.g. Fig. 5 at right).

Figure 5 at right exhibits the further surprising result that the H_3^+ abundance is largely independent of the cosmic ray ionization rate at early times when the H_2 abundance is small. This

occurs because formation of H_3^+ is a multistep process with a resultant inverse dependence on the electron density which may be much faster than linear (as suggested by Eq. (3)), combined with the tendency (suppressed but not eliminated by neutralization of atomic ions on small grains) for the ionization fraction to increase with ζ_H.

In a somewhat simplified form neglecting chemical reactions of H_2^+ and H_3^+ with neutral atoms etc. (appropriate in diffuse gas), and the complexities of grain neutralization, the main steps involved in forming and destroying H_3^+ and its immediate antecedent H_2^+ are:

$$\text{cosmic ray} + H_2 \rightarrow H_2^+ + e, \quad (4a)$$
$$H_2^+ + e \rightarrow 2H, \quad (4b)$$
$$H_2^+ + H_2 \rightarrow H_3^+ + H, \quad (4c)$$
$$H_3^+ + e \rightarrow 3H, \text{ etc.} \quad (4d)$$

So, whenever the recombination described in reaction 4b dominates over the protonation in reaction 4c, the abundance of H_2^+ will be inversely proportional to $n(e)$ and $n(H_3^+) \propto n(H_2)$ $n(H_2^+)/n(e) \propto \zeta_H/n(e)^2$. Calculating the ionization balance in an atomic gas according to the prescription in Spitzer (1978) indeed yields $n(e) \propto \sqrt{\zeta_H}$ for $\zeta_H \geq 10^{-17}$ s^{-1} under conditions typical of H I clouds.

For the model of a typical H I cloud shown at right in Fig. 5, such considerations are apparently sufficient to remove much of the dependence on ζ_H from the H_3^+ density at early times. To ascertain the conditions under which this effect is important, note that the recombination coefficient of H_2^+ is $\alpha = 4 \times 10^{-6}/\sqrt{T_K}$ cm^3 s^{-1} and reaction 4c proceeds with a rate constant $k = 2.08 \times 10^{-9}$ cm^3 s^{-1} in the UMIST database, see Le Teuff et al. (2000) or `http://www.rate99.co.uk`. Thus for $T_K = 100$ K and taking $n(e)$ as a small multiple (2×) of the gas-phase abundance of carbon, $n(C^+) \approx 1.4 \times 10^{-4} n(H)$, it follows that recombination dominates and the functional dependence of $n(H_3^+)$ upon ζ_H is weakened for $n(H_2)/n(H) \lesssim 0.05$, with higher H_2 concentrations required for higher $n(e)$ and/or ζ_H. In Fig. 5 at right, this is case for the first $1-2 \times 10^6$ yr.

4.3. Influence of H_3^+ on other trace molecule abundances

In general the surprisingly high abundance of H_3^+ in diffuse gas should not alter significantly the patterns of abundance of other trace species under the quiescent conditions discussed here, and it will certainly not by itself explain such outstanding mysteries as the high abundances of CH^+, NH, HCO^+, etc. For the former, the reaction $C + H_3^+ \rightarrow CH^+ + H_2$ is exothermic but not particularly fast and the fraction of gas-phase carbon which is neutral is very small in diffuse gas, typically below 1%: this forms only miniscule amounts of CH^+ (more CH^+ might be formed by the reaction of C with H_2^+). For NH (Crawford & Williams 1997; Meyer & Roth 1991), the reaction of N and H_3^+ is endothermic. For HCO^+, which in dark clouds is formed via the reaction $H_3^+ + CO \rightarrow HCO^+ + H_2$, the amounts of both H_3^+ and CO are too small in diffuse clouds to sustain HCO^+ against its recombination to CO, $HCO^+ + e \rightarrow CO + H_2$. CO can form from HCO^+ in quiescent diffuse gas (Liszt & Lucas 2000), but not the other way around.

One species for which H_3^+ might make a difference is OH, because both the reactions $O + H_3^+ \rightarrow OH^+ + H_2$ (rate constant $k_1 = 8 \times 10^{-10}$ cm^3 s^{-1}) and $O^+ + H_2 \rightarrow OH^+ + H$ (rate constant $k_2 = 1.7 \times 10^{-9}$ cm^3 s^{-1}) are exothermic. Figure 6 shows the time evolution of the volume formation rate of OH^+ through both routes (shown are $k_1 n(O) n(H_3^+)$ and $k_2 n(O^+) n(H_2)$) in three

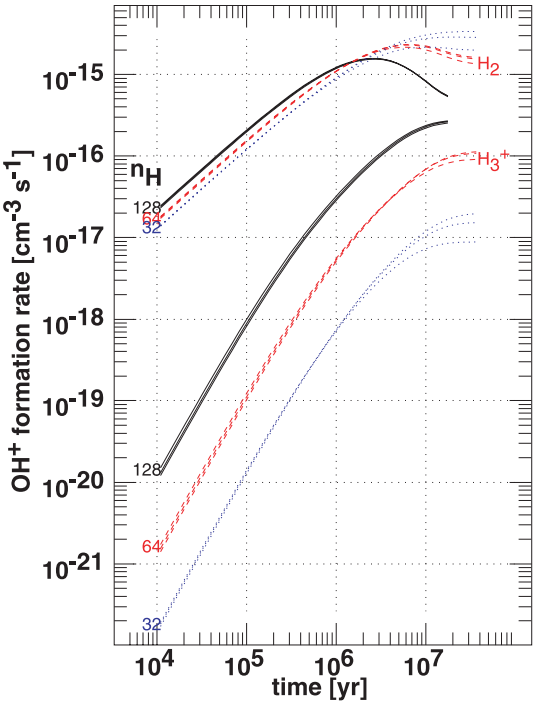

Fig. 6. OH^+ volume formation rates due to reaction of $O^+ + H_2$ (upper family of curves) and $O + H_3^+$ (lower family) in the presence of a high primary cosmic ray ionization rate $\zeta_H = 3 \times 10^{-16}$ s^{-1}. Results are shown at the usual three fractional radii within models of diameter 4.05 pc having $n(H) = 32$ cm^{-3}, 64 cm^{-3} and 128 cm^{-3}, so that $N(H) = 4 \times 10^{20}$ cm^{-2}, 8×10^{20} cm^{-2} and 16×10^{20} cm^{-2}, respectively.

models threaded by a high cosmic ray flux, $\zeta_H = 3 \times 10^{-16}$ s^{-1}, at three densities $n(H) = 32$ cm^{-3}, 64 cm^{-3} and 128 cm^{-3}. The cloud diameter is held fixed so that $N(H) = 4 \times 10^{20}$ cm^{-2}, 8×10^{20} cm^{-2} and 16×10^{20} cm^{-2}, respectively, purposely driving the highest density gas to very high H_2 fractions and H_3^+ abundances at late times.

As shown in Fig. 6, the reaction of O and H_3^+ is never a dominant source of OH^+. The figure does show, however, the effect of ionization balance on the OH formation rate (see also Sect. 2.3 of Liszt 2003): at later times the first step toward OH formation occurs more vigorously in the more tenuous models because their higher ionization levels (both overall and in oxygen) more than compensate for lower H_2 fractions. In the models with larger H_2 fractions, the proton density declines at late times because a more nearly molecular gas cannot sustain a high proton density and the O^+/O ratio also declines, due partly to its rapid charge exchange reaction with hydrogen and because of its rapid reaction with H_2. The cosmic-ray ionization alone, even at the high rates assumed here, cannot support high ionization fractions in atomic hydrogen or oxygen in the presence of PAH and high H_2 concentrations.

The next (necessary) step toward OH formation, $OH^+ + H_2 \rightarrow OH_2^+ + H$ will dominate over recombination of the OH^+ ion for H_2-fractions as small as 2% at diffuse cloud temperatures. Thus, the thinner models will actually form OH more rapidly (not just OH^+), as the H_2 accumulation process equilibrates[2]. Chemical effects like those shown in Fig. 6 undoubtedly contribute to the appearance of radio frequency

[2] At early times, the formation of OH in less dense clouds will be seriously impeded by their larger e/H_2 ratios and the denser models may make more OH. As with H_3^+ itself, high OH abundances only appear at the conclusion of the H_2 accumulation process.

OH emission in the envelopes of dark clouds well outside the most strongly molecular regions (see Wannier et al. 1993; and Fig. 6 of Liszt & Lucas 1996). In the current context we expect/predict that regions of higher than normal OH abundance should be found optically in diffuse clouds having modest extinction and H_2 fractions.

5. Summary and discussion

5.1. Summary

We showed the approach to equilibrium under benign conditions for some recently-published models (Liszt & Lucas 2000; Liszt 2002, 2003), calculating the time-dependent H_2 and H_3^+ formation in pc-size, otherwise largely static gas parcels meant to represent typical quiescent diffuse "clouds". We pointed out that self-shielding does not hasten the formation or accumulation of H_2, although it may foster the production of *more* H_2 over longer times. Because the H_2 formation process in diffuse gas is incomplete, timescales can in general not be deduced from simple scaling arguments based on the local H_2 formation rate. The equilibrium H_2 formation timescale in an H I cloud having a column density $N(\mathrm{H}) \approx 4\times10^{20}$ cm^{-2} is $1-3\times10^7$ yr, nearly independent of the assumed density or H_2 formation rate on grains, etc. Under the benign conditions described here, the bulk of the H_2 formation in the diffuse ISM actually occurs under diffuse conditions in physically larger regions of moderate density; that is, there is little apparent advantage in hypothesizing a process which forms H_2 in denser clumps, if the density remains within the range inferred for quiescent diffuse gas.

Other species reach equilibrium essentially as soon as H_2 does, even when they involve higher-order and/or very "slow" processes (like cosmic ray ionization of H_2) but their equilibrium abundances appear more nearly at just the last minute; it is more critical for explaining H_3^+ that conditions equilibrate than, say, for H_2 itself. This is also relevant because the chemistry of a weakly-molecular gas – which could be either a model of low density or one of higher density at early time – behaves in various particular ways. For instance, the predicted abundance of H_3^+ is less strongly dependent on the cosmic-ray ionization rate when $n(\mathrm{H_2})/n(\mathrm{H}) \lesssim 0.05$.

Attempts to form increased amounts of H_3^+ may be thwarted at very high assumed values of ζ_H both because the fractional ionization increases and because the H_2-fraction declines as cosmic-ray ionization overtakes photodissociation as the main H_2-destruction mechanism. Assuming $\zeta_\mathrm{H} \gg 10^{-16}$ s^{-1} will also change the thermal balance in the diffuse ISM as a whole as cosmic-ray ionization becomes the dominant heating process in both warm and cold neutral diffuse gas. Although observations of both HD and H_3^+ seem to indicate an enhanced low-level source of hydrogen ionization, it is important to ascertain whether it is indeed a cosmic-ray related process which is responsible (or some other form of very hard radiation) and whether any related effects occur in other phases of the interstellar medium, either in the warm or dark gas.

The presence of relatively high H_3^+ abundances per se probably does not have strong effects on the chemistry of other trace species whose abundances are puzzling (CH^+, NH, HCO^+ etc.) or on those of species like OH which are generally considered to be better understood. However, in considering competition between OH formation paths through H_2 and H_3^+, we showed that late-time OH formation proceeds most vigourously in more diffuse regions having modest density, extinction and H_2 fraction and somewhat higher fractional ionization, suggesting that high OH abundances might be found optically in diffuse clouds having modest extinction.

5.2. Lifetimes of diffuse clouds and their H_2

In this work we modelled the formation and accumulation of H_2 under conditions like those which are inferred from observations of the H_2 and related neutral gas species themselves; temperatures from H_2 (Savage et al. 1977; Shull et al. 2004) and mean thermal pressures (densities) from C I (Jenkins & Tripp 2001). Although modest amounts of H_2 form quickly enough that molecule-free sightlines are relatively rare, the observed high mean molecular fractions of 25−40% (Savage et al. 1977; Liszt & Lucas 2002) are achieved only over timescales of 10^7 yr or longer, when starting from scratch.

H_2 aside, timescales for thermal, ionization, chemical etc. equilibrium are short (Spitzer 1978; Wolfire et al. 2003; Rawlings et al. 2002) and diffuse gas is not normally thought of as having much longevity in any particular form. The H I cloud spectrum evolves under the continual influences of cloud-cloud collisions, evaporation, passage of supernova blast waves and stellar wind shocks etc. (Chieze & Lazareff 1980) and in a 3-phase model of the diffuse ISM, gas in any particular volume element turns over on timescales shorter than 10^6 yr according to McKee & Ostriker (1977).

How then are high H_2 fractions and short diffuse gas lifetimes to be reconciled? This question has never really been considered when the overall structure of the diffuse ISM is modelled, but there are several alternatives. 1) The long equilibrium timescales under diffuse neutral conditions provide, in reverse, some resilience which might help pre-existing H_2 to weather the changes which occur. 2) Dark clouds have haloes (Wannier et al. 1993; Bensch 2006) and it has been suggested that the molecules supposedly seen in diffuse clouds are actually located around and exchanging material with dark clouds (Federman & Allen 1991); this may be true in some cases, but complex trace molecules are also seen along sightlines which are quite well separated from the nearest dark material (Liszt et al. 2002). 3) Perhaps most promisingly, turnover within diffuse neutral gas due to turbulence, rapidly cycling material through a very dense phase, may provide for much faster formation of H_2 and trace species (Glover & Mac Low 2005; Falgarone et al. 2005), establishing high molecular fractions from scratch on short timescales. The small fraction of neutral material which is observed to exist at very high pressure within diffuse clouds (Jenkins & Tripp 2001) and other aspects of small-scale structure in diffuse gas (Deshpande 2000) may perhaps also be understood in such terms.

Acknowledgements. The National Radio Astronomy Observatory is operated by Associated Universites, Inc. under a cooperative agreement with the US National Science Foundation. The calculations described here were mostly completed while the author was enjoying the hospitality of Bel 'Esperance and La Clemence in Geneva and the Hotel de la Paix in Lausanne. The author is grateful to the referee and the editor for several stimulating comments.

References

Bakes, E. L. O., & Tielens, A. G. G. M. 1994, ApJ, 427, 822
Bensch, F. 2006, A&A, 448, 1043
Chieze, J. P., & Lazareff, B. 1980, A&A, 91, 290
Cox, P., Güsten, R., & Henkel, C. 1988, A&A, 206, 108
Crawford, I. A., & Williams, D. A. 1997, MNRAS, 291, L53
Deshpande, A. A. 2000, MNRAS, 317, 199
Draine, B. T., & Sutin, B. 1987, ApJ, 320, 803
Falgarone, E., Pineau Des Forêts, G., Hily-Blant, P., & Schilke, P. 2005, in IAU Symp., ed. D. Lis, G. Blake, & E. Herbst, 105

Federman, S. R., & Allen, M. 1991, ApJ, 375, 157
Glover, S. C. O., & Mac Low, M.-M. 2005, in IAU Symp., ed. D. C. Lis, G. A. Blake, & E. Herbst, 160
Goldsmith, D. W., Habing, H. J., & Field, G. B. 1969, ApJ, 158, 173
Gry, C., Boulanger, F., Nehmé, C., et al. 2002, A&A, 391, 675
Jenkins, E. B. 2002, ApJ, 580, 938
Jenkins, E. B., & Tripp, T. M. 2001, ApJS, 137, 297
Jura, M. 1974, ApJ, 191, 375
Le Petit, F., Roueff, E., & Herbst, E. 2004, A&A, 417, 993
Le Teuff, Y. H., Millar, T. J., & Markwick, A. J. 2000, A&AS, 146, 157
Lee, H. H., Herbst, E., Pineau Des Forets, G., Roueff, E., & Le Bourlot, J. 1996, A&A, 311, 690
Liszt, H. 2002, A&A, 389, 393
Liszt, H. 2003, A&A, 398, 621
Liszt, H. S., & Lucas, R. 1995, A&A, 299, 847
Liszt, H. S., & Lucas, R. 1996, A&A, 314, 917
Liszt, H. S., & Lucas, R. 2000, A&A, 355, 333
Liszt, H., & Lucas, R. 2002, A&A, 391, 693
Liszt, H., Lucas, R., & Pety, J. 2002, A&A, 448, 253
Liszt, H., Lucas, R., & Black, J. H. 2004, A&A, 428, 117
Lucas, R., & Liszt, H. S. 1996, A&A, 307, 237
Lucas, R., & Liszt, H. S. 2000, A&A, 358, 1069
McCall, B. J., Hinkle, K. H., Geballe, T. R., et al. 2002, ApJ, 567, 391
McCall, B. J., Huneycutt, A. J., Saykally, R. J., et al. 2003, Nature, 422, 500
McKee, C. F., & Ostriker, J. P. 1977, ApJ, 218, 148
Meyer, D. M., & Roth, K. C. 1991, ApJ, 376, L49
Moore, E. M., & Marscher, A. P. 1995, ApJ, 452, 671
Nash, A. G. 1990, ApJS, 72, 303
Rawlings, J. M. C., Hartquist, T. W., Williams, D. A., & Falle, S. A. E. G. 2002, A&A, 391, 681
Savage, B. D., & Sembach, K. R. 1996, ARA&A, 34, 279
Savage, B. D., Drake, J. F., Budich, W., & Bohlin, R. C. 1977, ApJ, 216, 291
Shull, J. M., Anderson, K., Tumlinson, J., & FUSE Science Team. 2004, Am. Astron. Soc. Meeting, 204
Spitzer, L. 1978, Physical processes in the interstellar medium (New York: Wiley-Interscience), 333
Wannier, P. G., Andersson, B.-G., Federman, S. R., et al. 1993, ApJ, 407, 163
Weingartner, J. C., & Draine, B. T. 2001, ApJS, 134, 263
Wolfire, M. G., Hollenbach, D., McKee, C. F., Tielens, A. G. G. M., & Bakes, E. L. O. 1995, ApJ, 443, 152
Wolfire, M. G., McKee, C. F., Hollenbach, D., & Tielens, A. G. G. M. 2003, ApJ, 587, 278